Open source models for the parametric study of diffraction gratings in 2D/2.5D/3D with <code>ONELAB</code>

Guillaume Demésy*, André Nicolet and Frédéric Zolla

Aix-Marseille Université, CNRS, Centrale Marseille, Institut Fresnel UMR 7249, 13013 Marseille, France

November 8, 2022

 $^{^*}Contact: {\tt guillaume.demesy@fresnel.fr}$

Abstract

This technical note aims at presenting both theoretical and practical aspects of the diffraction grating ONELAB models¹.

The model grating2D.pro applies to so-called mono-dimensional grating, *i.e.* structures having one direction of invariance as shown in Fig. 0.1(a). Various geometries and materials can be handled or easily added. The two classical polarization cases, denoted here E^{\parallel} (also denoted TE in the literature) and H^{\parallel} (or TM), are addressed. These are scalar problems where a scalar Helmholtz equation is solved.

The model grating3D.pro applies to possibly skewed crossed gratings, which are 3D structures with two directions of periodicity as shown in Fig. 0.1(b). The output of both models consist in a full energy balance of the problem computed from the field maps. This is a vector problem where a vector Helmholtz equation is solved.

Finally, the conical incidence (2D geometry, 3D incidence, see Fig. 0.1(c)) is treated thanks to a mixed formulation.

These models are based on free the open source pieces of software Gmsh [Geu+09], GetDP [Dul+98] and their interface ONELAB. For more technical insights and a more complete bibliography, the reader is invited to refer to [Dem+07; Dem+09; Dem+10].

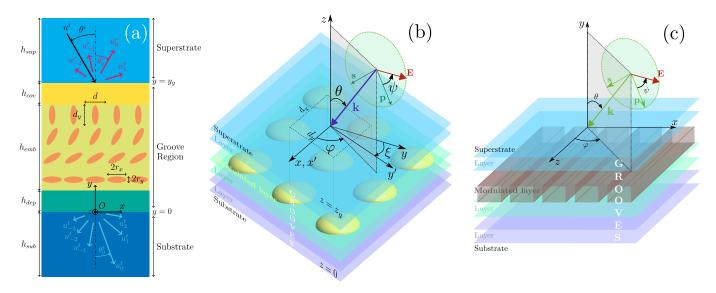


Figure 0.1: Scalar diffraction by a mono-dimensional grating (2D). (b) Vector diffraction by a crossed grating (3D). (c) Vector diffraction by a mono-dimensional grating (2.5D).

¹https://gitlab.onelab.info/doc/models/wikis/Diffraction-gratings

Contents

Contents				
1		ono-dimensional gratings: grating2D.pro	4	
	1.1	Intro		
	1.2	Theoretical model		
		1.2.1 Set up of the problem and notations		
		1.2.2 Appropriate diffracted field formulation		
	1.3	ONELAB model description		
		1.3.1 Geometry		
		1.3.2 Materials	13	
		1.3.3 Incident plane wave	15	
		1.3.4 Mesh size and PMLs parameters	15	
		1.3.5 Post plot options	16	
	1.4	Energy balance post-processing in python	16	
	1.5	Examples	16	
		1.5.1 General recommendations	16	
		1.5.2 Lamellar grating example	17	
		1.5.3 Anisotropic grating		
		1.5.4 Photonic crystal slab example		
		1.5.5 Resonant grating		
		1.5.6 Plasmonic grating		
	1.6	Conclusion		
2	Crossed gratings: grating3D.pro			
	2.1	Problem statement	24	
		2.1.1 Structure and notations		
		2.1.2 Incident plane wave		
		2.1.3 Problem statement		
	2.2	Scattered field formulation		
	2.3	The annex problem		
	2.4	Variational formulation		
	2.5	Energy balance: Diffraction efficiencies and losses		
	$\frac{2.5}{2.6}$	Total field formulation	31	
	$\frac{2.0}{2.7}$	Convergence	31	
	2.1	Convergence	91	
3	The	e conical 2.5D case	33	
Bi	Bibliography			

Chapter 1

Mono-dimensional gratings: grating2D.pro

1.1 Intro

This chapter aims at presenting both theoretical and practical aspects regarding the grating_2D ONELAB model, mainly for educational purposes. This model applies to so-called mono-dimensional grating, *i.e.* structures having one direction of invariance. Various geometries and materials can be handled or easily added. The two classical polarization cases, denoted here E^{\parallel} (or TE) and H^{\parallel} (or TM), are addressed. The output consists in a full energy balance of the problem computed from the field maps. For more detailed information and associated bibliography, the curious reader is invited refer to [Dem+07].

1.2 Theoretical model

1.2.1 Set up of the problem and notations

We denote by \mathbf{x} , \mathbf{y} and \mathbf{z} , the unit vectors of the axes of an orthogonal co-ordinate system Oxyz. Time-harmonic regime is assumed; consequently, the electric and magnetic fields are represented by the complex vector fields \mathbf{E} and \mathbf{H} with a time dependence chosen in $\exp(-i\omega t)$. We are now considering 2D structures 0z is the axis of invariance.

Besides, in this model, we assume that the tensor fields of relative permittivity ε_r and relative permeability μ_r can be written as follows:

$$\boldsymbol{\varepsilon}_{r} = \begin{pmatrix} \varepsilon_{xx} & \bar{\varepsilon}_{a} & 0\\ \varepsilon_{a} & \varepsilon_{yy} & 0\\ 0 & 0 & \varepsilon_{zz} \end{pmatrix} \quad \text{and} \quad \boldsymbol{\mu}_{r} = \begin{pmatrix} \mu_{xx} & \bar{\mu}_{a} & 0\\ \mu_{a} & \mu_{yy} & 0\\ 0 & 0 & \mu_{zz} \end{pmatrix} , \tag{1.1}$$

where $\varepsilon_{xx}, \varepsilon_a, \dots \mu_{zz}$ are possibly complex valued functions of the two variables x and y and where $\bar{\varepsilon}_a$ (resp. $\bar{\mu}_a$) represents the conjugate complex of ε_a (resp. μ_a). These kinds of materials are said to be z-anisotropic. It is of importance to note that with such tensor fields, lossy materials can be studied (the lossless materials correspond to tensors with real diagonal terms represented by Hermitian matrices) and that the problem is invariant along the z-axis but the tensor fields can vary continuously (gradient index gratings) or discontinuously (step index gratings). We define the wavenumber $k_0 := \omega/c$.

The gratings that we are dealing with are made of three regions (See Fig. 1.1a).

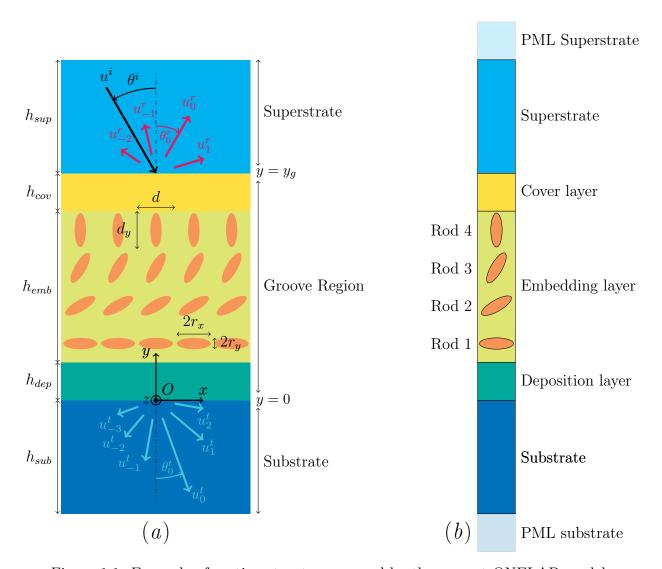


Figure 1.1: Example of grating structure covered by the present ONELAB model.

- The superstrate $(y > y_g)$ which is supposed to be homogeneous, isotropic and lossless and characterized solely by its real valued relative permittivity ε_r^+ and its relative permeability μ_r^+ . We denote $k^+ := k_0 \sqrt{\varepsilon_r^+ \mu_r^+}$.
- The substrate (y < 0) is supposed to be homogeneous and isotropic and therefore characterized by its relative permittivity ε_r^- and its relative permeability μ_r^- . We denote $k^- := k_0 \sqrt{\varepsilon_r^- \mu_r^-}$.
- The groove region $(0 < y < y_g)$ is heterogeneous and z-anisotropic. It is characterized by the two tensor fields $\varepsilon_r^g(x,y)$ and $\boldsymbol{\mu}_r^g(x,y)$. It is worth noting that the method presented in this paper does work irrespective of whether the tensor fields are piecewise constant. The grating periodicity along x-axis will be denoted d.

This grating is illuminated by an incident plane wave of wave vector

$$\mathbf{k}_{\perp}^{+} = \alpha \mathbf{x} - \beta^{+} \mathbf{y} = k^{+} \left(\sin \theta_{0} \mathbf{x} - \cos \theta_{0} \mathbf{y} \right),$$

whose electric field $(E^{\parallel}$ polarization case) (resp. magnetic field $(H^{\parallel}$)) is linearly polarized along the z-axis:

$$\mathbf{E}_{e}^{0} = \mathbf{A}_{e}^{0} \exp(i\mathbf{k}_{\downarrow}^{+} \cdot \mathbf{r}) \mathbf{z} \quad (\text{resp. } \mathbf{H}_{m}^{0} = \mathbf{A}_{m}^{0} \exp(i\mathbf{k}_{\downarrow}^{+} \cdot \mathbf{r}) \mathbf{z}) , \qquad (1.2)$$

where \mathbf{A}_e^0 (resp. \mathbf{A}_m^0) is an arbitrary complex number. The magnetic (resp. electric) field derived from \mathbf{E}_e^0 (resp. \mathbf{H}_m^0) is denoted \mathbf{H}_e^0 (resp. \mathbf{E}_m^0) and the electromagnetic field associated with the incident field is therefore denoted $(\mathbf{E}^0, \mathbf{H}^0)$ which is equal to $(\mathbf{E}_e^0, \mathbf{H}_e^0)$ (resp. $(\mathbf{E}_m^0, \mathbf{H}_m^0)$).

The problem of diffraction that we address in this paper is therefore to find Maxwell's equation solutions in harmonic regime *i.e.* the unique solution (\mathbf{E}, \mathbf{H}) of:

$$\begin{cases} \mathbf{curl} \ \mathbf{E} = +i\omega\mu_0 \,\boldsymbol{\mu}_r \mathbf{H} \\ \mathbf{curl} \ \mathbf{H} = -i\omega\varepsilon_0 \,\boldsymbol{\varepsilon}_r \mathbf{E} \end{cases}$$
 (1.3a)

such that the diffracted field satisfies an Outgoing Waves Condition (O.W.C. [Pet92; Pet80]) and where **E** and **H** are quasi-periodic functions with respect to the x co-ordinate.

1.2.2Appropriate diffracted field formulation

Decoupling of fields and z-anisotropy

We assume that $\delta(x,y)$ is a z-anisotropic tensor field ($\delta_{xz} = \delta_{yz} = \delta_{zx} = \delta_{zy} = 0$). Moreover, the left upper matrix extracted from δ is denoted δ , namely:

$$\widetilde{\boldsymbol{\delta}} = \begin{pmatrix} \delta_{xx} & \bar{\delta}_a \\ \delta_a & \delta_{yy} \end{pmatrix} . \tag{1.4}$$

For z-anisotropic materials, with non-conical incidence, the problem of diffraction can be split into two fundamental cases $(H^{\parallel} \text{ case and } E^{\parallel} \text{ case})$. This property results from the following equality which can be easily derived:

$$-\operatorname{\mathbf{curl}}\left(\boldsymbol{\delta}^{-1}\operatorname{\mathbf{curl}}\left(u\mathbf{z}\right)\right) = \operatorname{div}\left(\frac{\widetilde{\boldsymbol{\delta}}^{T}}{\det(\widetilde{\boldsymbol{\delta}})}\operatorname{\mathbf{\mathbf{grad}}}u\right)\mathbf{z},\tag{1.5}$$

where u is a function which does not depend on the z variable. From the previous equality, it appears that the non-conical problem of diffraction amounts to looking for an electric (resp. magnetic) field which is polarized along the z-axis; $\mathbf{E} = e(x,y)\mathbf{z}$ (resp. $\mathbf{H} = h(x,y)\mathbf{z}$). The functions e and h are therefore solutions of similar differential equations:

$$\mathcal{L}_{\boldsymbol{\xi},\chi}(u) := \operatorname{div}\left(\boldsymbol{\xi} \operatorname{\mathbf{grad}} u\right) + k_0^2 \chi \, u = 0 \tag{1.6}$$

with

$$u = e, \quad \boldsymbol{\xi} = \widetilde{\boldsymbol{\mu}}^T / \det(\widetilde{\boldsymbol{\mu}}), \quad \chi = \varepsilon_{zz} ,$$
 (1.7)

in the E^{\parallel} case and

$$u = h, \quad \boldsymbol{\xi} = \widetilde{\boldsymbol{\varepsilon}}^T / \det(\widetilde{\boldsymbol{\varepsilon}}), \quad \chi = \mu_{zz} ,$$
 (1.8)

in the H^{\parallel} case.

Reducing the diffraction problem to a radiation problem with localized sources

In its initial form, the problem of diffraction summed up by Eq. (1.6) is not well suited to the Finite Element Method. We propose to split the unknown function u into a sum of two functions u_1 and u_2^d , the first term being known as a closed form and the latter being a solution of a radiation problem whose sources are localized within the obstacles. This is, in essence, a diffracted field formulation extended to the case where the substrate and superstrate are made of different materials.

We have assumed that outside the groove region (cf. Fig. 1.1), the tensor field $\boldsymbol{\xi}$ and the function χ are constant and equal respectively to $\boldsymbol{\xi}^-$ and χ^- in the substrate (y < 0) and equal respectively to $\boldsymbol{\xi}^+$ and χ^+ in the superstrate $(y > y_g)$. Besides, for the sake of clarity, the superstrate is supposed to be made of an isotropic and lossless material and is therefore solely defined by its relative permittivity ε_r^+ and its relative permeability μ_r^+ , which leads to:

$$\boldsymbol{\xi}^+ = \frac{1}{\mu_r^+} \operatorname{Id}_2 \quad \text{and} \quad \chi^+ = \varepsilon_r^+ \quad \text{in } H^{\parallel} \text{ case}$$
 (1.9)

or

$$\boldsymbol{\xi}^{+} = \frac{1}{\varepsilon_r^{+}} \operatorname{Id}_2 \quad \text{and} \quad \chi^{+} = \mu_r^{+} \quad \text{in } E^{\parallel} \text{ case}, \tag{1.10}$$

where Id_2 is the 2×2 identity matrix. With such notations, $\pmb{\xi}$ and χ are therefore defined as follows:

$$\boldsymbol{\xi}(x,y) := \begin{cases} \boldsymbol{\xi}^{+} & \text{for } y > y_{g} \\ \boldsymbol{\xi}^{g}(x,y) & \text{for } y_{g} > y > 0 \\ \boldsymbol{\xi}^{-} & \text{for } y < 0 \end{cases}, \ \chi(x,y) := \begin{cases} \chi^{+} & \text{for } y > y_{g} \\ \chi^{g}(x,y) & \text{for } y_{g} > y > 0 \\ \chi^{-} & \text{for } y < 0 \end{cases}.$$
(1.11)

It is now apropos to introduce an auxiliary tensor field ξ_1 and an auxiliary function χ_1 :

$$\boldsymbol{\xi}_{1}(x,y) := \begin{cases} \boldsymbol{\xi}^{+} & \text{for } y > 0 \\ \boldsymbol{\xi}^{-} & \text{for } y < 0 \end{cases}, \ \chi_{1}(x,y) := \begin{cases} \chi^{+} & \text{for } y > 0 \\ \chi^{-} & \text{for } y < 0 \end{cases},$$
 (1.12)

these quantities corresponding, of course, to a simple plane interface. Besides, we introduce the constant tensor field ξ_0 which is equal to ξ^+ everywhere and a constant scalar field χ_0 which is equal to χ^+ everywhere. Finally, we denote u_0 the function which equals the incident field u^{inc} in the superstrate and vanishes elsewhere:

$$u_0(x,y) := \begin{cases} u^{\text{inc}} & \text{for } y > y_g \\ 0 & \text{for } y < y_g \end{cases}$$
 (1.13)

We are now in a position to reformulate the diffraction problem of interest. The function u is the unique solution of

$$\mathcal{L}_{\boldsymbol{\xi},\chi}(u) = 0$$
 such that $u^d := u - u_0$ satisfies an O.W.C. (1.14)

In order to reduce this problem of diffraction to a radiation problem, an intermediate function is necessary. This function, called u_1 , is defined as the unique solution of the equation:

$$\mathscr{L}_{\boldsymbol{\xi}_1,\chi_1}(u_1) = 0$$
 such that $u_1^d := u_1 - u_0$ satisfies an O.W.C. (1.15)

The function u_1 corresponds thus to an annex problem associated to a simple interface and can be solved in closed form and from now on is considered as a known function. As written above, we need the function u_2^d which is simply defined as the difference between u and u_1 :

$$u_2^d := u - u_1 = u^d - u_1^d . (1.16)$$

The presence of the superscript d is, of course, not irrelevant: As the difference of two diffracted fields, the O.W.C. of u_2^d is guaranteed (which is of prime importance when dealing with PML cf. 1.2.2). As a result, the Eq. (1.14) becomes:

$$\mathcal{L}_{\xi,\chi}(u_2^d) = -\mathcal{L}_{\xi,\chi}(u_1) , \qquad (1.17)$$

where the right hand member is a scalar function which may be interpreted as a known source term $-\mathcal{S}_1(x,y)$ and the support of this source is localized only within the groove region. To prove it, all we have to do is to use Eq. (1.15):

$$\mathscr{S}_1 := \mathscr{L}_{\boldsymbol{\xi},\chi}(u_1) = \mathscr{L}_{\boldsymbol{\xi},\chi}(u_1) - \underbrace{\mathscr{L}_{\boldsymbol{\xi}_1,\chi_1}(u_1)}_{=0} = \mathscr{L}_{\boldsymbol{\xi}-\boldsymbol{\xi}_1,\chi-\chi_1}(u_1) . \tag{1.18}$$

Now, let us point out that the tensor fields $\boldsymbol{\xi}$ and $\boldsymbol{\xi}_1$ are identical outside the groove region and the same holds for χ and χ_1 . The support of \mathscr{S}_1 is thus localized within the groove region as expected. It remains to compute more explicitly the source term \mathscr{S}_1 . Making use of the linearity of the operator \mathscr{L} and the equality $u_1 = u_1^d + u_0$, the source term can be split into two terms:

$$\mathscr{S}_1 = \mathscr{S}_1^0 + \mathscr{S}_1^d \,, \tag{1.19}$$

where

$$\mathscr{S}_1^0 = \mathscr{L}_{\boldsymbol{\xi} - \boldsymbol{\xi}_1, \chi - \chi_1}(u_0) \tag{1.20}$$

and

$$\mathscr{S}_1^d = \mathscr{L}_{\boldsymbol{\xi} - \boldsymbol{\xi}_1, \chi - \chi_1}(u_1^d) . \tag{1.21}$$

Now, since u_0 is nothing but a plane wave $u_0 = \exp(i\mathbf{k}^+_{\downarrow} \cdot \mathbf{r})$ (with $\mathbf{k}^+_{\downarrow} = \alpha \mathbf{x} - \beta^+ \mathbf{y}$), it is sufficient to give $\mathbf{grad} u_0 = i\mathbf{k}^+_{\downarrow} u_0$ for the weak formulation associated with Eq. (1.17):

$$\mathscr{S}_{1}^{0} = \left\{ i \operatorname{div} \left[\left(\boldsymbol{\xi}^{+} - \boldsymbol{\xi} \right) \mathbf{k}_{\downarrow}^{+} \exp(\mathbf{k}_{\downarrow}^{+} \cdot \mathbf{r}) \right] + k_{0}^{2} \left(\chi^{+} - \chi \right) \exp(i \mathbf{k}_{\downarrow}^{+} \cdot \mathbf{r}) \right\} . \tag{1.22}$$

The same holds for the term associated with the diffracted field $(u_1^d = \rho \exp(i\mathbf{k}^+_{\uparrow} \cdot \mathbf{r}))$, with $(\mathbf{k}^+_{\uparrow} = \alpha \mathbf{x} + \beta^+ \mathbf{y})$:

$$\mathscr{S}_{1}^{d} = \rho \left\{ i \operatorname{div} \left[\left(\boldsymbol{\xi}^{+} - \boldsymbol{\xi} \right) \mathbf{k}_{\uparrow}^{+} \exp(i \mathbf{k}_{\uparrow}^{+} \cdot \mathbf{r}) \right] + k_{0}^{2} \left(\chi^{+} - \chi \right) \exp(i \mathbf{k}_{\uparrow}^{+} \cdot \mathbf{r}) \right\} , \tag{1.23}$$

where ρ is nothing but the complex reflection coefficient associated with the simple interface :

$$\rho = \frac{p^{+} - p^{-}}{p^{+} + p^{-}} \text{ with } p^{\pm} = \begin{cases} \beta^{\pm} \text{ in the } E^{\parallel} \text{ case} \\ \frac{\beta^{\pm}}{\varepsilon_{r}^{\pm}} \text{ in the } H^{\parallel} \text{ case} \end{cases}$$
(1.24)

An important remark about the choice of the unknown diffracted field

It is important to understand that we have several choices for the unknown field. Our goal is to formulate an equivalent problem for which the support of the sources is bounded and inside the computational domain.

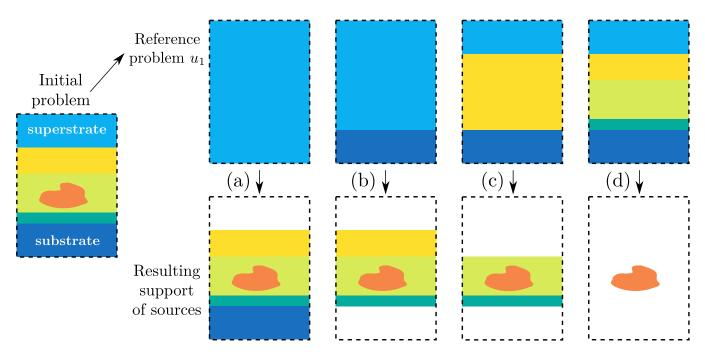


Figure 1.2: Some possible choices for the annex problem.

Figure 1.2 illustrates the impact of the choice of the annex problem upon the support of the sources. With choice (a), the annex problem is nothing but the response of freespace to the desired incident field, which is trivial to compute indeed. However, the corresponding scattering problem (see bottom inset) has now sources in the substrate which is unbounded. So we didn't gain much here: Instead of solving for the total field with sources inside the unbounded superstrate, we now have to solve a scattered field with sources in the unbounded substrate. We understand here the importance of considering a total field and an annex field satisfying the same radiation condition both inside the substrate and the superstrate. Choices (b,c,d) in Figure 1.2 are more suitable candidates since they take into account the impedance mismatch between the superstrate and the substrate. Choice (b) amounts to nothing but compute the Fresnel coefficients of the planar interface. For choices (c,d), one has to compute first the response of a multilayer.

When considering periodic structures, the simplest choice is choice (b) and this is the choice made throughout this document. However, note that when considering isolated scatterers embedded in a multilayer, we need to extend the discussion to consider the "lateral" radiation condition in order to avoid incoming sources from an infinite distance along x in the scattering problem. The only choice is then choice (d), where one has to pre-compute the field scattered by the 1D invariant multilayered stack.

Quasi-periodicity and weak formulation

The weak formulation follows the classical lines and is based on the construction of a weighted residual of Eq. (1.6), which is multiplied by the complex conjugate of a weight function u' and integrated by part to obtain:

$$\mathscr{R}_{\boldsymbol{\xi},\chi}(u,u') = \int_{\Omega} -(\boldsymbol{\xi} \operatorname{\mathbf{grad}} u) \cdot \overline{\operatorname{\mathbf{grad}} u'} + k_0^2 \chi u \, \overline{u'} \, \mathrm{d}\Omega + \int_{\partial\Omega} \overline{u'} \, (\boldsymbol{\xi} \operatorname{\mathbf{grad}} u) \cdot \mathbf{n} \, \mathrm{d}\ell$$
 (1.25)

The solution u of the weak formulation can therefore be defined as the element of the space $H^1(\mathbf{grad}, d, \alpha)$ of quasi-periodic functions (i.e. such that $u(x,y) = u_{\#}(x,y)e^{ikx}$ with $u_{\#}(x,y) = u_{\#}(x+d,y)$, a d-

periodic function and where both u and $\operatorname{grad} u$ are square integrable) such that:

$$\mathscr{R}_{\boldsymbol{\xi},\chi}(u,u') = 0 \ \forall u' \in H^1(\mathbf{grad},d,\alpha). \tag{1.26}$$

As for the boundary term introduced by the integration by part, it can be classically set to zero at the PML endings by imposing Dirichlet conditions on a part of the boundary (the value of u is imposed and the weight function u' can be chosen equal to zero on this part of the boundary) or by imposing homogeneous Neumann conditions ($\boldsymbol{\xi} \operatorname{\mathbf{grad}} u$) $\cdot \mathbf{n} = 0$ on another part of the boundary (and u is therefore an unknown to be determined on the boundary). A third possibility (applied here to lateral boundaries) are the so-called quasi-periodicity conditions of particular importance in the modeling of gratings. Denote by Γ_l and Γ_r the lines parallel to the y-axis delimiting a cell of the grating respectively from its left and right neighbor cell. Considering that both u and u' are in $L^2(\operatorname{\mathbf{curl}}, d, k)$, the boundary term for $\Gamma_l \cup \Gamma_r$ is

$$\int_{\Gamma_l \cup \Gamma_r} \overline{u'} \left(\boldsymbol{\xi} \ \mathbf{grad} \ u \right) \cdot \mathbf{n} dS = \int_{\Gamma_l \cup \Gamma_r} \overline{u'_\#} e^{-ikx} \left(\boldsymbol{\xi} \ \mathbf{grad} (u_\# e^{+ikx}) \right) \cdot \mathbf{n} dS =$$

$$\int_{\Gamma_l \cup \Gamma_r} \overline{u'_\#} \left(\boldsymbol{\xi} \left(\mathbf{grad} \ u_\# + iku_\# \mathbf{x} \right) \right) \cdot \mathbf{n} dS = 0$$

because the integrand $\overline{u'_{\#}}$ ($\boldsymbol{\xi}$ (grad $u_{\#} + iku_{\#}\mathbf{x}$)) · \mathbf{n} is periodic along x and the normal \mathbf{n} has opposite directions on Γ_l and Γ_r so that the contributions of these two boundaries have the same absolute value with opposite signs. The contribution of the boundary terms vanishes therefore naturally in the case of quasi-periodicity.

The finite element method is based on this weak formulation and both the solution and the weight functions are classically chosen in a discrete space made of linear or quadratic Lagrange elements, i.e. piecewise first or second order two variable polynomial interpolation built on a triangular mesh of the domain Ω (cf. Fig.1.1b). Dirichlet and Neumann conditions may be used to truncate the PML domain in a region where the field (transformed by the PML) is negligible. The quasi-periodic boundary conditions are imposed by considering the u as unknown on Γ_l (in a way similar to the homogeneous Neumann condition case) while, on Γ_r , u is forced equal to the value of the corresponding point on Γ_l (i.e. shifted by a quantity -d along x) up to the factor $e^{i\alpha d}$. The practical implementation in the finite element method is described in details in Ref. [Zol+12].

Perfectly Matched Layers

The main drawback encountered in electromagnetism when tackling theory of gratings through the finite element method is the non-decreasing behaviour of the propagating modes in superstrate and substrate (if those are made of lossless materials): The PML has been introduced by berenger94perfecmatch-layer in order to get round this obstacle. Standard PMLs constant profile are implemented in the present model.

Post-processing: Diffraction efficiencies calculation

The rough result of the FEM calculation is the total complex field solution of Eq. (1.6) at each point of the bounded domain. We deduce from u^d (cf Eq. (1.14)) the diffraction efficiencies with the following method. The superscripts $^+$ (resp. $^-$) correspond to quantities defined in the superstrate (resp. substrate) as previously.

On the one hand, since u^d is quasi-periodic along the x-axis, it can be expanded as a Rayleigh expansion (see for instance [Pet92; Pet80]):

for
$$y < 0$$
 and $y > y_g$, $u^d(x, y) = \sum_{n \in \mathbb{Z}} u_n^d(y) e^{i\alpha_n x}$, (1.27)

where

$$u_n^d(y) = \frac{1}{d} \int_{-d/2}^{d/2} u^d(x, y) e^{-i\alpha_n x} dx \text{ with } \alpha_n = \alpha + \frac{2\pi}{d} n.$$
 (1.28)

On the other hand, introducing Eq. (1.27) into Eq. (1.6) leads to the Rayleigh coefficients:

$$u_n^d(y) = \begin{cases} s_n e^{+i\beta_n^+ y} + r_n e^{-i\beta_n^+ y} & \text{for } y > y_g \\ u_n e^{-i\beta_n^- y} + t_n e^{+i\beta_n^- y} & \text{for } y < 0 \end{cases} \text{ with } \beta_n^{\pm^2} = k^{\pm^2} - \alpha_n^2$$
 (1.29)

For a temporal dependence in $e^{+i\omega t}$, the O.W.C. imposes $s_n = u_n = 0$. Combining Eq. (1.28) and Eq. (1.29) at a fixed y_0 altitude leads to:

$$\begin{cases}
r_n = \frac{1}{d} \int_{-d/2}^{d/2} u^d(x, y_0) e^{-i(\alpha_n x - \beta_n^+ y_0)} dx & \text{for } y_0 > y_g \\
t_n = \frac{1}{d} \int_{-d/2}^{d/2} u^d(x, y_0) e^{-i(\alpha_n x + \beta_n^- y_0)} dx & \text{for } y_0 < 0
\end{cases}$$
(1.30)

We extract these two coefficients by numerical integration along x from a cut of the previously calculated field map at altitudes $y_0 = -h_{sub}$ in the substrate and $y_0 = y_g + h_{sup}$ in the superstrate. From this we immediately deduce the reflected and transmitted diffracted efficiencies of propagative orders $(T_n \text{ and } R_n)$ defined by:

$$\begin{cases}
R_n := r_n \overline{r_n} \frac{\beta_n^+}{\beta^+} & \text{for } y_0 > y_g \\
T_n := t_n \overline{t_n} \frac{\beta_n^-}{\beta^-} \frac{\gamma^+}{\gamma^-} & \text{for } y_0 < 0
\end{cases} \text{ with } \gamma^{\pm} = \begin{cases}
1 \text{ in the } E^{\parallel} \text{ case} \\
\varepsilon_r^{\pm} \text{ in the } H^{\parallel} \text{ case}
\end{cases}$$
(1.31)

1.3 ONELAB model description

In this section, the parameters of the ONELAB model are briefly commented in their order of appearance in the gmsh's left panel.

1.3.1 Geometry

Grating period

• |value| grating period [nm] allows to set the period d of the grating given in nanometers.

Stack thicknesses

The following parameters can take any positive float value.

- value substrate thickness [nm] allows to set h_{subs} , given in nanometers. Quantitative results should not depend on this parameter since the substrate is by definition a half plane.
- value deposit layer thickness [nm] allows to set h_{dep} , given in nanometers.
- value cover layer thickness [nm] allows to set h_{cov} , given in nanometers.
- value superstrate thickness [nm] allows to set h_{sup} , given in nanometers. Quantitative results should not depend on this parameter since the superstrate is by definition a half plane.

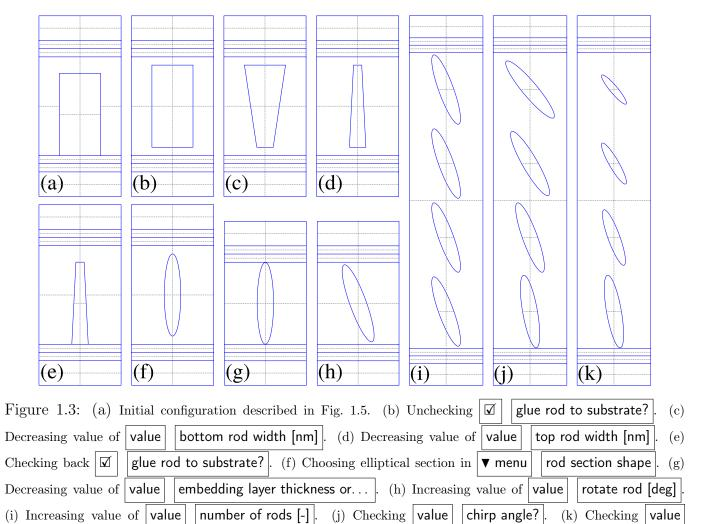
Note that h_{emb} is set by the diffractive element dimensions detailed hereafter.

Diffractive element dimensions

In order to illustrate the various grating or photonic crystal slabs covered by this model, let us start from the lamellar grating situation shown in Fig. 1.5:

- 🗹 glue rod to substrate? having the element relying directly on the substrate changes the topology, it needs to be specified. The checking/unchecking of this box is illustrated in Figs. 1.3(a-b) and (d-e).
- menu rod section shape Choose between elliptical or trapezoidal rod section. See Figs. 1.3(e-f).
- value number of rods [-] Integer value setting the number of rods to consider along y axis spaced by d_y (see below). See Figs. 1.3(h-i).
- value bottom rod width [nm] In case of a trapezoidal rod, this value sets the bottom width Figs. 1.3(c). In case of an elliptical rod, this value has no effect. See Figs. 1.3(b-c).
- value top rod width [nm] In case of a trapezoidal rod, this value sets the top width Figs. 1.3(c). In case of an elliptical rod, this value sets its diameter $(2r_x)$. See Figs. 1.3(c-d).
- value rod thickness [nm] In case of a trapezoidal rod, this value sets the thickness (dimension along y). In case of an elliptical rod, this value sets its diameter $(2r_y)$.
- value embedding layer thickness or "period" along y if number of rods >1, [nm] If the number of rods is set to 1, this value sets h_{emb} . In case of several rods, this value sets their periodic spacing along $y(d_y)$. See Figs. 1.3(i).
- value rotate rod [deg] Rotates the rod around himself (axis formed by its barycenter, the Oz direction). See Figs. 1.3(g-h).

- value chirp angle? In case of several rods, the rotation angle of the next rod along increasing values of y is increased by the value described in the previous item. See Figs. 1.3(i-j).
- value chirp size factor [%]
- \square chirp size? In case of several rods, the size of the next rod along increasing values of y is scaled of the value given in the previous item. See Figs. 1.3(j-k).



1.3.2 Materials

chirp size ? | and decreasing | value

Dispersive materials

For each constitutive layer, a choice of materials is proposed. The file <code>grating_2D_materials.pro</code> contains frequency dispersion tables for some selected materials. Relative permittivity values are linearly interpolated using these tables. The available materials are currently:

chirp size factor [%]

• Air: freespace

1. MONO-DIMENSIONAL GRATINGS: grating2D.pro

- SiO2 : silicon dioxide
- Ag (palik) : silver, values from Ref. [Pal98]
- Al (palik) : aluminium, values from Ref. [Pal98]
- Au (johnson): gold, values from Ref. [Joh+72]
- Nb2O5 : niobium pentoxide, values from Ref. [Pol]
- ZnSe : zinc selenide, values from Ref. [Pol]
- MgF2 : magnesium fluoride, values from Ref. [Pol]
- TiO2: titanium dioxide, values from Ref. [Pol]
- PMMA : methyl polymethacrylate, values from Ref. [Pol]
- | Si | : silicon, values from Ref. [Pal98]
- ITO: indium tin oxide, values from Ref. [Pol]
- Cu (palik) : copper, values from Ref. [Pal98]
- | custom 1 | : custom dispersion free material, see next section
- custom 2: custom dispersion free material, see next section
- | custom 3 | : custom dispersion free material, see next section

It is easy to add another material, instructions are given in comments at the beginning of the file grating_2D_materials.pro.

Custom non-dispersive materials

Another possibility is to set a material permittivity to custom 1, custom 2, or custom 3 in which case the real and imaginary parts of the complex relative permittivity will be set to the one manually specified in this section. Beware that due to the $-i\omega t$ time dependence, the imaginary part of passive (lossy) materials is **positive**. Finally, the so-called permittivity of the rods (and the rods only) can be z-anisotropic, i.e. of the form given in Eq. (1.1).

- 🗹 Enable anisotropy for rods? If checked, the permittivity of the rods (and the rods only) will be z-anisotropic with values given below. Checking this will override material rods above.
- ullet value epsilonr XX re $\operatorname{sets} \, \Re e\{arepsilon_{xx}\}$

- ullet value epsilonr XX im sets $\Im m\{arepsilon_{xx}\}$
- ullet value epsilonr YY re $\operatorname{sets} \, \Re e\{arepsilon_{yy}\}$
- $\bullet \quad | \text{value} \quad | \text{ epsilonr YY im} \quad \text{sets } \Im m\{\varepsilon_{yy}\}$
- ullet value epsilonr ZZ re sets $\Re e\{arepsilon_{zz}\}$
- ullet value epsilonr ZZ im sets $\Im m\{arepsilon_{zz}\}$
- ullet value epsilonr XY re sets $\Re e\{arepsilon_{xy}\}$
- value epsilonr XY im sets $\Im m\{\varepsilon_{xy}\}$

Note that so-called z-anisotropy means for the relative permittivity tensor that $\varepsilon_{xz} = \varepsilon_{yz} = \varepsilon_{zx} = \varepsilon_{zy} = 0$ and that $\varepsilon_{yx} = \overline{\varepsilon_{xy}}$.

1.3.3 Incident plane wave

- value wavelength [nm] sets the operating freespace wavelength λ_0 of the incident plane wave.
- value incident plane wave angle [deg] sets the angle of incidence θ^i of the incident plane wave.
- wmenu polarization case allows to select the (scalar) H^{\parallel} or E^{\parallel} polarization cases (see Eq. (1.2)), or the conical 2.5D case (see Chap. 3).
- value number of post-processed diffraction orders sets the number of diffraction orders to be post-processed (e.g. if set to 2, five Fourier coefficients will be computed corresponding to diffraction orders -2,-1,0,+1,+2)

1.3.4 Mesh size and PMLs parameters

- value top PML size [nm] allows to set the top PML thickness. Typically, it should not be set to a value smaller than $\lambda_0/2$ while a value larger than $3\lambda_0$ is pointless; λ_0 is usually a reasonable value with the default PML complex stretch.
- value bottom PML size [nm] allows to set the top PML thickness. Typically, it should not be set to a value smaller than $\lambda_0/2$ while a value larger than $3\lambda_0$ is pointless; λ_0 is usually a reasonable value with the default PML complex stretch.
- value nb of mesh elements per wavelength [-] sets the average number of triangles used to discretize one freespace wavelength (mesh refinement). Typically, setting it to 30 offers 4 or 5 significant digits over energy related quantities while setting it to 1 leads to very wrong results...

• Custom Mesh parameters: When dealing with metals and/or very small objects, it is sometimes necessary to locally refine the mesh in the affected subdomain, which can be prescribed in this section. For instance, Figs. 1.4 shows a local refinement of the rods. In Fig. 1.4(a), the mesh is very coarse, its typical size is $\lambda_0/6$ everywhere. The mesh size within the rods in Fig. 1.4(b) is 3 times smaller $(\lambda_0/(6\times3))$.

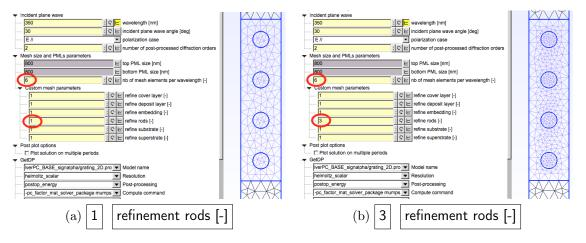


Figure 1.4: Mesh refinement options.

1.3.5 Post plot options

• \square Plot solution on multiple periods. If checked, the field $(E_z(x,y))$ in E^{\parallel} polarization case, $H_z(x,y)$ in H^{\parallel} polarization case) is post-processed over 9 grating periods cells, as shown in Fig. 1.5. The field in a neighboring cell is indeed nothing but the field in the reference cell up to a phase shift $e^{\pm i\alpha d}$.

1.4 Energy balance post-processing in python

The provided file grating_2D_postplot.py gives a possible representation of energy related quantities. If only a single ONELAB run was made, it provides bar plot of non-null absorption, reflection and transmission. If a parametric ONELAB run was made, e.g. a spectrum, it provides a plot of non-null absorption, reflection and transmission.

1.5 Examples

In this section, various example of the literature are retrieved.

1.5.1 General recommendations.

The ONELAB model internal files, grating_2D.geo and grating_2D.pro. Both call a configuration file named grating_2D_data.geo setting all the parameters displayed in the gmsh left panel. Thus in order to load directly one of the provided configurations, just rename grating_2D_data_someconfig.geo to grating_2D_data.geo (and grating_2D_data.geo to grating_2D_data_old.geo). Then, open grating_2D.pro

with gmsh. It is advised to clean the working directory between two different study. To do so, remove at least the output directory run_results and the mesh file grating_2d.msh need to be deleted. Rarely, the Bloch boundary condition fails and getdp will complain not finding twin nodes on the two boundaries. Just change the mesh parameter a little and ... remesh. Finally, if you are not satisfied with the numerical precision, try to refine the mesh and/or increase the size of the PMLs.

1.5.2 Lamellar grating example.

The LamellarGrating example (parameter file grating_2D_data_LamellarGrating.geo) reproduces some results found in lower half of Table n°2 in [Gra99].

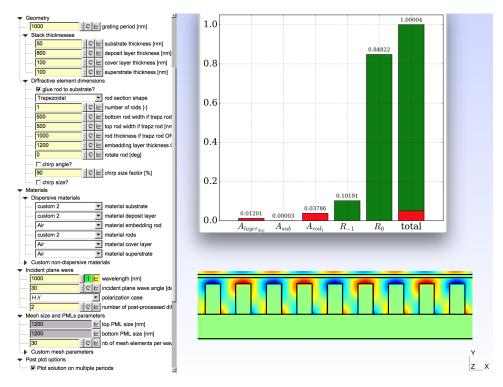


Figure 1.5: Lamellar grating example. The bar plot shows the output of grating_2D_postplot.py.

At least three significant digits are obtained on the diffraction efficiencies.

1.5.3 Anisotropic grating

The AnisotropicGrating example (parameter file grating_2D_data_AnisotropicGrating.geo) illustrates the numerical results in [Dem+07]. Figure 1.6 shows the field map $\Re e\{E_z\}$ in V/m for an angle of incidence $\theta^i = -20^\circ$. There is no anisotropic behavior here since E_z only "sees" ε_{zz} Figure 1.7 shows the field map $\Re e\{H_z\}$ in A/m for an angle of incidence $\theta^i = 0^\circ$. The lack of symmetry due to the anisotropy of the scatterer is clearly visible here.

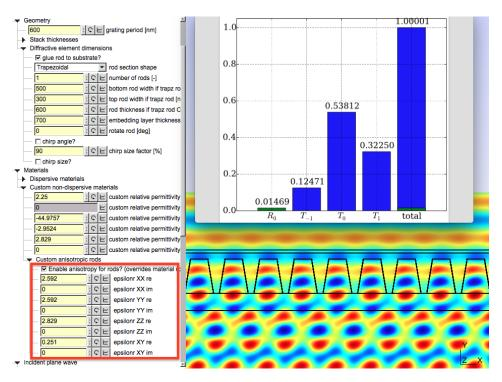


Figure 1.6: H^{\parallel} case. See Fig. 5b and 6^{th} line of Tab. 2 in reference [Dem+07].

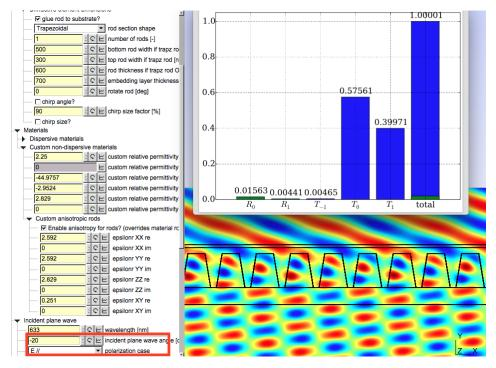


Figure 1.7: E^{\parallel} case. See Fig. 5c and third line of Tab. 2 in reference [Dem+07].

1.5.4 Photonic crystal slab example.

This PhotonicCrystalSlab example (parameter file grating_2D_data_PhotonicCrystalSlab.geo) illustrates some results found in the textbook [joannopoulos2008molding] (see Fig. 2, page 68). In this example, the band structure of a 2D photonic crystal is given in the two polarization cases. The

 E^{\parallel} case features a full photonic bandgap. As a consequence, a sufficiently thick slice of this infinite crystal is expected to exhibit good reflecting properties for an incident plane wave with frequency within the bandgap. The photonic crystal is made of circular rods of diameter 0.4a with relative permittivity $\varepsilon_r = 8.9$ arranged in a square lattice with lattice constant a, with background relative permittivity $\varepsilon_r = 1$. The E^{\parallel} gap is found to be roughly in the normalized frequency $\omega a/2\pi c$ range [0.3, 0.43]. In other words, setting in the period d to 150 nm should place the bandgap in the wavelength range [440, 660] nm. The gap is total so the reflection on a slab with a few lattices should lead to high reflection for any angle of incidence.

As depicted in Fig. 1.8(a), for an angle of incidence $\theta^i = 30^\circ$, a very high reflection coefficient is obtained for $N_{rods} = 5$ only. The python program grating_2D_postplot.py produces the figure in Fig. 1.8(b).

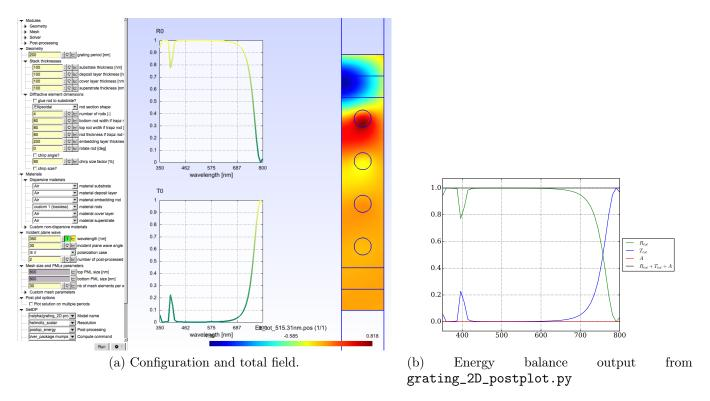


Figure 1.8: Photonic crystal slab example.

Finally, one wonders the slab thickness necessary to witness a high reflectivity (*i.e.* how many periods in y do we need to see the gap?). A possible parametric study is possible by simply:

- unchecking "looping over" λ_0 [10] , setting it to $\lambda_0 = 500 \, \text{nm}$,
- checking "looping over" N_{rods} : \bigcirc , setting looping parameters : to 1:10:1

Figure 1.9 shows in log scale the transmission coefficient decaying exponentially with photonic crystal slab thickness. This is expected given the evanescent nature of the field inside photonic crystal slab.

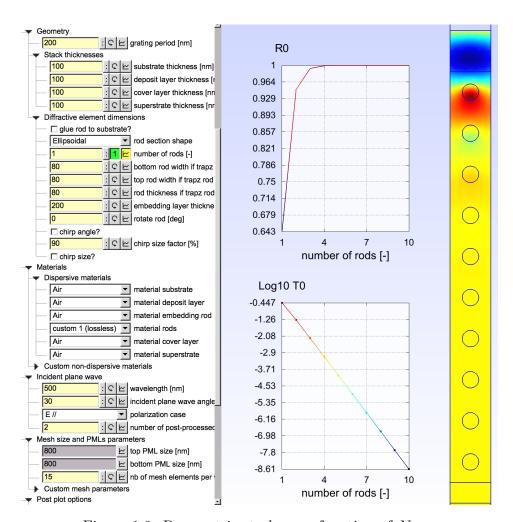


Figure 1.9: Parametric study as a function of N_{rods} .

1.5.5 Resonant grating

The ResonantGrating example (parameter file grating_2D_data_ResonantGrating.geo) illustrates the behavior of resonant grating that can be used to obtain a very sharp spectral response as detailed in Ref. [Feh+02].

Spectral response

The spectral response of such a grating is depicted in Fig. 1.10.

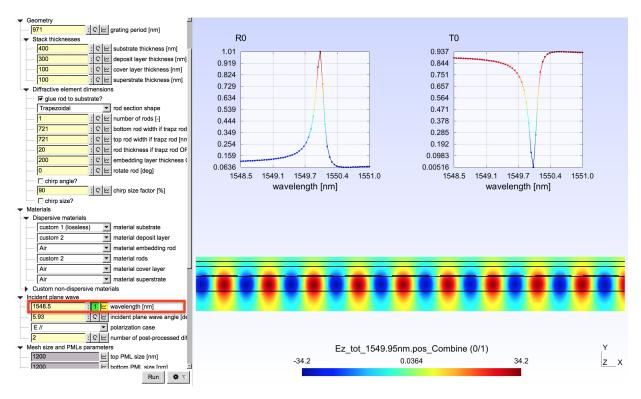


Figure 1.10: Spectral response.

Angular response

From the very same model up to a few preliminary clicks, one can obtain the angular response of the filter by:

- unchecking "looping over" λ_0 , setting it to $\lambda_0 = 1550.05 \,\mathrm{nm}$: 1550.05 wavelength [nm]
- checking "looping over" θ^i : 6 incident plane wave angle [deg]
- setting the looping parameters for θ^i from 5.85° to 6.0° by 0.0025° steps using the button and filling 5.85:6:0.0025.

The angular response of this grating is depicted in Fig. 1.11.

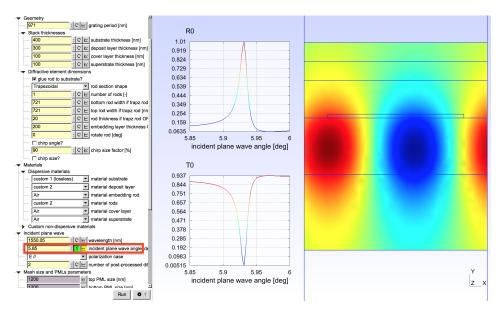


Figure 1.11: Angular response.

1.5.6 Plasmonic grating

The example in grating_2D_data.geo has no other purpose than to show that the model handles exotic so-called plasmonic configurations. The detailed energy balance associated to this weird silver structure in Fig. 1.12 shows an equilibrated repartition of the energy occurring inside losses in each rod, reflection and transmission in both specular and non-specular diffraction efficiencies.

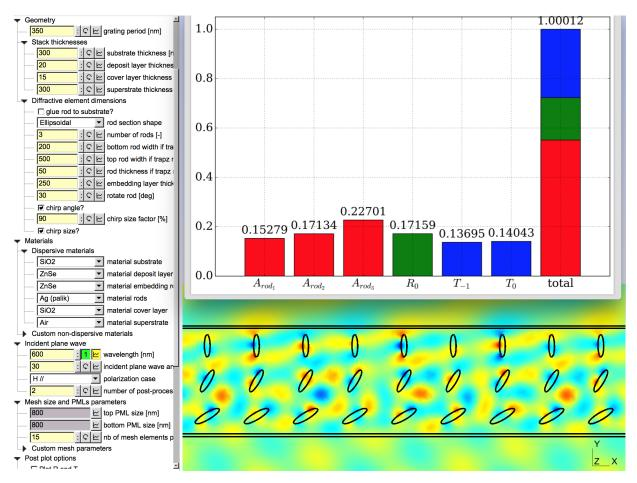


Figure 1.12: Plasmonic grating.

1.6 Conclusion

This model is a general tool for the study of so-called mono-dimensional grating. Various geometries and materials can be handled or easily added. For instance, it can be easily adapted to nano-structured solar cells. The two classical polarization cases, denoted here E^{\parallel} and H^{\parallel} , are addressed. The output consists in a full energy balance of the problem computed from the field maps.

Chapter 2

Crossed gratings: grating3D.pro

2.1 Problem statement

2.1.1 Structure and notations

We denote by $\hat{\mathbf{x}}$, $\hat{\mathbf{y}}$ and $\hat{\mathbf{z}}$ the unit vectors of the axes of an orthogonal coordinate system Oxyz. We only deal with time-harmonic fields; consequently, electric and magnetic fields are represented by the complex vector fields \mathbf{E} and \mathbf{H} , with a time dependance in $\exp(-i\omega t)$. Besides, in this section, for the sake of simplicity, the substrate and superstrate are assumed to be isotropic. It is of importance to note that lossy materials can be studied, the relative permittivity and relative permeability being represented by complex valued functions. As detailed in the introduction of this chapter, the annex problem allowing to define a proper scattered field formulation is the diopter one, schematically depicted in Fig. 1.2(b). Consequently, the tensor fields $\boldsymbol{\varepsilon}_r$ and $\boldsymbol{\mu}_r$ fully characterizing the optogeometric characteristics of the crossed-gratings we are dealing with (see Fig. 2.1 where each color represents possibly distinct materials) can be defined by part over the following regions:

- The superstrate $(z > z_g)$ is supposed to be homogeneous, isotropic and lossless, and therefore characterized its relative permittivity $\varepsilon_{r,1}$ and its relative permeability $\mu_{r,1}$ and we denote $k_1 := k_0 \sqrt{\varepsilon_{r,1}\mu_{r,1}}$, where $k_0 := \omega/c$,
- The groove region $(0 < z < z_g)$, which is possibly heterogeneous and/or anisotropic. The relative permittivity and permeability can vary continuously (gradient index gratings) or discontinuously (step index gratings). It means that the groove region can be constituted of a multilayer stack for instance. This region is thus characterized by the tensor fields $\boldsymbol{\varepsilon}_r^g(\mathbf{x})$ and $\boldsymbol{\mu}_r^g(\mathbf{x})$. The groove periodicity along the x-axis, respectively (resp.) y'-axis, is denoted d_x , resp. d_y .
- The substrate (z < 0) is supposed to be homogeneous and isotropic and therefore characterized by its relative permittivity $\varepsilon_{r,2}$ and its relative permeability $\mu_{r,2}$ and we denote $k_2 := k_0 \sqrt{\varepsilon_{r,2}\mu_{r,2}}$,

In short, we have defined:

$$\boldsymbol{\varepsilon}_{r}(\mathbf{x}) = \begin{cases} \varepsilon_{r,1} \, \mathbb{1} & \text{for } z > z_{g} \\ \boldsymbol{\varepsilon}_{r}^{g}(\mathbf{x}) & \text{for } z \in [0, z_{g}] \\ \varepsilon_{r,2} \, \mathbb{1} & \text{for } z < 0 \end{cases} \quad \text{and } \boldsymbol{\mu}_{r}(\mathbf{x}) = \begin{cases} \boldsymbol{\mu}_{r,1} \, \mathbb{1} & \text{for } z > z_{g} \\ \boldsymbol{\mu}_{r}^{g}(\mathbf{x}) & \text{for } z \in [0, z_{g}] \\ \boldsymbol{\mu}_{r,2} \, \mathbb{1} & \text{for } z < 0 \end{cases}$$
 (2.1)

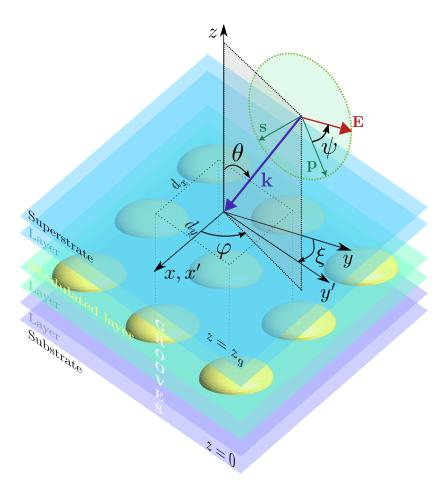


Figure 2.1: Scheme of the crossed grating and angles convention for the incident plane wave.

2.1.2 Incident plane wave

The incident field on this structure is denoted:

$$\mathbf{E}^{\text{inc}} = \mathbf{A}_0^e \exp(i\,\mathbf{k}_1 \cdot \mathbf{x}) \tag{2.2}$$

with

$$\mathbf{k}_{1} = \begin{bmatrix} k_{x} \\ k_{y} \\ k_{z,1} \end{bmatrix} = k_{1} \begin{bmatrix} -\sin \theta_{0} \cos \varphi_{0} \\ -\sin \theta_{0} \sin \varphi_{0} \\ -\cos \theta_{0} \end{bmatrix}. \tag{2.3}$$

The vector amplitude \mathbf{A}_0^e allows to controle the polarization nature of the plane wave (linear defined by the angle ψ_0 , circular or elliptical) will be specified later on.

Remark

The plane wave E^{inc} is bi-quasi-periodic in the skewed basis. In order to proove it and incidentally to determine the relevant Bloch phase shifts, it is sufficient to derive $\mathbf{E}^{\mathrm{inc}}(\mathbf{x} + d_x \hat{\mathbf{x}})$ and $\mathbf{E}^{\mathrm{inc}}(\mathbf{x}+d_{u}\hat{\mathbf{y}}')$:

•
$$\mathbf{E}^{\text{inc}}(\mathbf{x} + d_x \hat{\mathbf{x}}) = \mathbf{A}_0^e \exp(i \, \mathbf{k}_1 \cdot \mathbf{x}) \exp(i \, d_x \, \mathbf{k}_1 \cdot \hat{\mathbf{x}}) = e^{i \, d_x \, k_1^x} \, \mathbf{E}^{\text{inc}}(\mathbf{x})$$

•
$$\mathbf{E}^{\mathrm{inc}}(\mathbf{x} + d_y \hat{\mathbf{y}}') = \mathbf{A}_0^e \exp(i \, \mathbf{k}_1 \cdot \mathbf{x}) \exp\left[(i \, d_y \mathbf{k}_1 \cdot (\cos \, \xi \hat{\mathbf{x}} + \sin \, \xi \hat{\mathbf{y}})\right]$$

= $\exp\left[-i \, d_y \, k_1 \sin \, \theta_0 \, \sin(\varphi_0 + \xi)\right] \, \mathbf{E}^{\mathrm{inc}}(\mathbf{x})$

These phase shifts will be used in the quasi-periodicity constraints. Note that when ξ vanishes, one retrieves the usual phase shift $e^{i d_y k_1^y}$ along the y direction.

2.1.3 Problem statement

We recall here the diffraction problem: Finding the solution of Maxwell equations in harmonic regime *i.e.* the unique solution (\mathbf{E}, \mathbf{H}) of:

$$\begin{cases} \operatorname{curl} \mathbf{E} = i\omega\mu_0 \,\boldsymbol{\mu}_r \,\mathbf{H} \\ \operatorname{curl} \mathbf{H} = -i\omega\varepsilon_0 \,\boldsymbol{\varepsilon}_r \,\mathbf{E} \end{cases} \tag{2.4a}$$

$$\operatorname{curl} \mathbf{H} = -i\omega\varepsilon_0 \,\boldsymbol{\varepsilon}_r \,\mathbf{E} \tag{2.4b}$$

such that the diffracted field satisfies the so-called Outgoing Waves Condition (OWC) and where **E** and **H** are quasi-bi-periodic functions with respect to x and y' coordinates. One can choose to compute arbitrarily E, or H since one can be deduced from the other at the cost and associated numerical of a spatial differenciation. Finally, the diffraction problem amounts to looking for the unique solution E of the so-called vector Helmholtz propagation equation, deduced from Eqs. (2.4a,2.4b):

$$\begin{cases}
-\operatorname{curl}\left[\boldsymbol{\mu}_{r}^{-1}\operatorname{curl}\mathbf{E}\right] + k_{0}^{2}\,\boldsymbol{\varepsilon}_{r}\,\mathbf{E} = \mathbf{0} \\
\text{with } \mathbf{E}_{:}^{d} = \mathbf{E} - \mathbf{E}_{0} \text{ outgoing} \\
\text{and } \mathbf{E} \text{ quasi-periodic along } (Ox) \text{ and } (Oy')
\end{cases}$$
(2.5)

where \mathbf{E}_0 coincides with $\mathbf{E}^{\mathrm{inc}}$ in the superstrate and the groove regions and vanishes in the substrate.

2.2Scattered field formulation

The annex problem allowing to define a suitable scattered field formulation can now be introduced. It corresponds to the problem of a simple plane diopter which is the same problem as before if we consider the grove region filled with the same material as the superstrate. We introduce the tensor fields corresponding to this diopter:

$$\boldsymbol{\varepsilon}_{r,a}(\mathbf{x}) = \begin{cases} \varepsilon_{r,1} \, \mathbb{1} & \text{for } z > 0 \\ \varepsilon_{r,2} \, \mathbb{1} & \text{for } z < 0 \end{cases} \text{ and } \boldsymbol{\mu}_{r,a}(\mathbf{x}) = \begin{cases} \mu_{r,1} \, \mathbb{1} & \text{for } z > 0 \\ \mu_{r,2} \, \mathbb{1} & \text{for } z < 0 \end{cases}.$$
 (2.6)

We are looking for the unique solution \mathbf{E}_1 of:

$$\begin{cases}
-\operatorname{curl}\left[\boldsymbol{\mu}_{r,a}^{-1}\operatorname{curl}\mathbf{E}_{1}\right] + k_{0}^{2}\,\boldsymbol{\varepsilon}_{r,a}\,\mathbf{E}_{1} = \mathbf{0} \\
\text{with } \mathbf{E}_{1}^{d} := \mathbf{E}_{1} - \mathbf{E}_{0} \text{ outgoing}
\end{cases}$$
(2.7)

Now the only difficulty is to obtain a closed form for \mathbf{E}_1 in our 3D setting, where it is trivial in 2D since we are talking about the Fresnel coefficients of the diopter. This will be detailed in the last paragraph.

As explained in the introduction of this chapter, the actual unknown of the problem is a field \mathbf{E}_2^d defined as the difference between \mathbf{E} and \mathbf{E}_1 and we have: $\mathbf{E}_2^d = \mathbf{E} - \mathbf{E}_1 = \mathbf{E}^d - \mathbf{E}_1^d$. It is important to note that \mathbf{E}_2^d satisfies the same outgoing condition as \mathbf{E}^d and \mathbf{E}_1^d . Again, this is a guarantee that no source will be present in the regions with infinite extent in the scattered field formulation. Finally, making use of the definition of \mathbf{E}_2^d and of the two vector Helmholtz defined above, the propagation equation satisfied by can be easily obtained:

$$-\operatorname{curl}\left[\boldsymbol{\mu}_{r}^{-1}\operatorname{curl}\mathbf{E}_{2}^{\mathrm{d}}\right] + \frac{\omega^{2}}{c^{2}}\boldsymbol{\varepsilon}_{r}\mathbf{E}_{2}^{\mathrm{d}} = \frac{\omega^{2}}{c^{2}}(\boldsymbol{\varepsilon}_{r,a} - \boldsymbol{\varepsilon}_{r})\mathbf{E}_{1} - \operatorname{curl}\left[\left(\boldsymbol{\mu}_{r,a}^{-1} - \boldsymbol{\mu}_{r}^{-1}\right)\operatorname{curl}\mathbf{E}_{1}\right],$$
(2.8)

where the right-hand side is a quasi-bi-periodic source term with support in the whole groove region solely.

2.3 The annex problem

In order to be useful in the context of the FEM, one need to obtain an analytical or semi-analytical expression for the solution of the annex problem. To that extent, we make use of the Fresnel coefficients of course. The assumption of considering isotropic substrate and superstrate is crucial here. It would be possible to consider anisotropic substrates and superstrates, but it would substantially complexify the notions of diffraction efficiencies, outgoing wave conditions and PMLs, incident field and polarization.

The field \mathbf{E}_1 can be relatively easily obtained in the basis formed by the two traditional $(\hat{\mathbf{p}}, \hat{\mathbf{s}})$ polarization cases, where the following convention is chosen: $\hat{\mathbf{s}} := [\sin \varphi_0, -\cos \varphi_0, 0]^T$ and $\hat{\mathbf{p}} := \hat{\mathbf{s}} \times \mathbf{k}_1/k_1$, as shown in green color in Fig. 2.1, so that $(\hat{\mathbf{p}}, \hat{\mathbf{s}}, \mathbf{k}_1/k_1)$ form a direct orthonormal basis. But first, one needs to introduce the wave vectors of the transmitted (\mathbf{k}_2) and reflected fields (\mathbf{k}_1^r) :

$$\mathbf{k}_{1}^{r} = \begin{bmatrix} k_{x} \\ k_{y} \\ -k_{z,1} \end{bmatrix} \text{ and } \mathbf{k}_{2} = \begin{bmatrix} k_{x} \\ k_{y} \\ k_{z,2} \end{bmatrix}. \tag{2.9}$$

with $k_{z,2} = -\sqrt{k_0^2 \,\varepsilon_{r,2} \,\mu_{r,2} - k_x^2 - k_y^2}$.

The Fresnel coefficients are classically given by:

$$\begin{cases}
 r_s = \frac{k_{z,1} - k_{z,2}}{k_{z,1} + k_{z,2}} & \text{and} \quad t_s = \frac{2k_{z,1}}{k_{z,1} + k_{z,2}} \\
 r_p = \frac{k_{z,1} \varepsilon_{r,2} - k_{z,2} \varepsilon_{r,1}}{k_{z,1} \varepsilon_{r,2} + k_{z,2} \varepsilon_{r,1}} & \text{and} \quad t_p = \frac{2k_{z,1} \varepsilon_{r,2}}{k_{z,1} \varepsilon_{r,2} + k_{z,2} \varepsilon_{r,1}}
\end{cases}$$
(2.10)

From the Fresnel coefficients, one can readily right the expressions of the fully \hat{s} -polarized electric and magnetic fields :

$$\begin{cases}
\mathbf{E}_{\hat{\mathbf{s}}}^{i} = \exp[i\mathbf{k}_{1} \cdot \mathbf{x}] \,\hat{\mathbf{s}} \\
\mathbf{E}_{\hat{\mathbf{s}}}^{r} = r_{s} \exp[i\mathbf{k}_{1}^{r} \cdot \mathbf{x}] \,\hat{\mathbf{s}} \\
\mathbf{E}_{\hat{\mathbf{s}}}^{t} = t_{s} \exp[i\mathbf{k}_{2} \cdot \mathbf{x}] \,\hat{\mathbf{s}}
\end{cases}$$
and
$$\begin{cases}
\mathbf{H}_{\hat{\mathbf{s}}}^{i} = 1/Z_{1} \exp[i\mathbf{k}_{1} \cdot \mathbf{x}] \,\hat{\mathbf{s}} \\
\mathbf{H}_{\hat{\mathbf{s}}}^{r} = r_{p}/Z_{1} \exp[i\mathbf{k}_{1}^{r} \cdot \mathbf{x}] \,\hat{\mathbf{s}} \\
\mathbf{H}_{\hat{\mathbf{s}}}^{t} = t_{p}/Z_{1} \exp[i\mathbf{k}_{2} \cdot \mathbf{x}] \,\hat{\mathbf{s}}
\end{cases}$$
(2.11)

with
$$Z_1 = \sqrt{\mu_0/(\varepsilon_0 \varepsilon_{r,1})}$$
.

The purely $\hat{\mathbf{p}}$ -polarized electric field can be deduced from the $\hat{\mathbf{s}}$ magnetic field:

$$\begin{cases}
\mathbf{E}_{\hat{\mathbf{p}}}^{i} = -\mathbf{k}_{1} \times \mathbf{H}_{\hat{\mathbf{s}}}^{i} / (\omega \varepsilon_{0} \varepsilon_{r,1}) \\
\mathbf{E}_{\hat{\mathbf{p}}}^{r} = -\mathbf{k}_{1}^{r} \times \mathbf{H}_{\hat{\mathbf{s}}}^{r} / (\omega \varepsilon_{0} \varepsilon_{r,1}) \\
\mathbf{E}_{\hat{\mathbf{p}}}^{t} = -\mathbf{k}_{2} \times \mathbf{H}_{\hat{\mathbf{s}}}^{t} / (\omega \varepsilon_{0} \varepsilon_{r,2})
\end{cases} (2.12)$$

Finally, the two elementary electric fields polarized solution to the diopter problem as $\mathbf{E}_{1\hat{\mathbf{s}}}$ and $\mathbf{E}_{1\hat{\mathbf{p}}}$ as :

$$\mathbf{E}_{1\{\hat{\mathbf{s}},\hat{\mathbf{p}}\}} = \begin{cases} \mathbf{E}_{\{\hat{\mathbf{s}},\hat{\mathbf{p}}\}}^{i} + \mathbf{E}_{\{\hat{\mathbf{s}},\hat{\mathbf{p}}\}}^{r} & \text{for } z > 0 \\ \mathbf{E}_{\{\hat{\mathbf{s}},\hat{\mathbf{p}}\}}^{t} & \text{for } z < 0 \end{cases}$$

$$(2.13)$$

In the end,

one can conveniently define a linearly polarized plane wave or a circular (left of right) on the bases formed by the $(E_{1\hat{\mathbf{s}}}, E_{1\hat{\mathbf{p}}})$ fields :

• linear with amplitude A_e with angle ψ_0 with respect to the plane of incidence (see Fig. 2.1) :

$$\mathbf{E}_1 = A_e \left(\cos \psi_0 \,\mathbf{E}_{1\hat{\mathbf{p}}} - \sin \psi_0 \,\mathbf{E}_{1\hat{\mathbf{s}}}\right) \tag{2.14}$$

• circular right or left with amplitude A_e :

$$\mathbf{E}_{1} = \frac{A_{e}}{\sqrt{2}} \left(\mathbf{E}_{1\hat{\mathbf{p}}} \pm i \, \mathbf{E}_{1\hat{\mathbf{s}}} \right) \tag{2.15}$$

Note that this choice is heavily dictated by the fact that the FEM software GetDP nicely handles the notion of vector fields defined by part and the cross-product between them.

2.4 Variational formulation

The variational form residue is obtained by multiplying scalarly Eq. (2.8) by weighted vectors **W** chosen among the ensemble of quasi-periodic square integrable fields with square integrable **curl**, denoted $H^1(\Omega, \mathbf{curl}, (d_x \hat{\mathbf{x}}, d_y \hat{\mathbf{y}}'), \mathbf{k})$. The variational diffraction problem reads as follows.

Find \mathbf{E}_2^d such that $\forall \mathbf{W} \in H^1(\Omega, \mathbf{curl}, (d_x \hat{\mathbf{x}}, d_y \hat{\mathbf{y}}'), \mathbf{k})$

$$-\int_{\Omega} \boldsymbol{\mu}_{r}^{-1} \operatorname{curl} \mathbf{E}_{2}^{d} \cdot \overline{\operatorname{curl} \mathbf{W}} \, d\Omega + k_{0}^{2} \int_{\Omega} \boldsymbol{\varepsilon}_{r} \, \mathbf{E}_{2}^{d} \cdot \overline{\mathbf{W}} \, d\Omega$$

$$-k_{0}^{2} \int_{\Omega_{g}} (\boldsymbol{\varepsilon}_{r,a} - \boldsymbol{\varepsilon}_{r}) \, \mathbf{E}_{1} \cdot \overline{\mathbf{W}} \, d\Omega$$

$$+ \int_{\Omega_{g}} (\boldsymbol{\mu}_{r,a}^{-1} - \boldsymbol{\mu}_{r}^{-1}) \, \operatorname{curl} \mathbf{E}_{1} \cdot \overline{\operatorname{curl} \mathbf{W}} \, d\Omega$$

$$+ \int_{\partial\Omega_{g}} \left(\mathbf{n}_{\text{ext}} \times \left((\boldsymbol{\mu}_{r,a}^{-1} - \boldsymbol{\mu}_{r}^{-1}) \operatorname{curl} \mathbf{E}_{1} \right) \right) \cdot \overline{\mathbf{W}} \, d\Gamma$$

$$- \int_{\Gamma_{\text{PML}}^{+} \cup \Gamma_{\text{PML}}^{-}} \left(\mathbf{n}_{\text{ext}} \times (\boldsymbol{\mu}_{r}^{-1} \operatorname{curl} \mathbf{E}_{2}^{d}) \right) \cdot \overline{\mathbf{W}} \, d\Gamma$$

$$= 0.$$
(2.16)

The last three terms are usually null at optical frequencies: The two terms involving a contrast of permeability are usually null for amagnetic problems, while the very last term arising from the integration by part of the **curl** affects the behavior of the field at the PML endings. There are two obvious choices regarding this boundary term: The first one is to force it to zero (homogeneous Neumann condition, perfect magnetic conductor) by simply forgetting it from the formulation, the second one to assume that the tangential components of the field are null at the PML endings by choosing test function null at the PML endings (Dirichlet condition, perfect electric conductor). The first option should be considered if possible because knowing the values of the field at PML endings allows to assess the efficiency of the PML implemented. The advantage of the second option is that it leads to smaller discrete systems since there are no unknowns at the PML endings.

From a discrete point of view, the first term in Eq. 2.16 leads to the so-called stiffness matrix, the second term to the mass matrix while the third term leads to the load vector.

2.5 Energy balance: Diffraction efficiencies and losses

In order to define the diffraction efficiencies, one needs to introduce the components of the wavevectors of the corresponding plane waves :

$$\begin{cases}
\alpha_{m,n} = -k_x + \frac{2\pi}{d_x} m \\
\beta_{m,n} = -k_y + \frac{1}{\cos \xi} \frac{2\pi}{d_y} n - \tan \xi \frac{2\pi}{d_x} m \\
\gamma_{m,n}^r = \sqrt{k_0^2 \varepsilon_{r,1} - \alpha_{m,n}^2 - \beta_{m,n}^2} \\
\gamma_{m,n}^t = \sqrt{k_0^2 \varepsilon_{r,2} - \alpha_{m,n}^2 - \beta_{m,n}^2}
\end{cases}$$
(2.17)

The classical Rayleigh expansion provides the complex amplitude of each diffraction order:

$$\begin{cases}
e_{m,n}^{r,u} = \frac{1}{d_x d_y \cos \xi} \int_{\Gamma^+} \exp\left[i(\alpha_{m,n} x + \beta_{m,n} y)\right] \mathbf{E}^{\mathbf{d}} \cdot \hat{\mathbf{u}} \, dS \\
e_{m,n}^{t,u} = \frac{1}{d_x d_y \cos \xi} \int_{\Gamma^-} \exp\left[i(\alpha_{m,n} x + \beta_{m,n} y)\right] \mathbf{E} \cdot \hat{\mathbf{u}} \, dS
\end{cases},$$
(2.18)

with u spans $\{x, y, z\}$ and $\hat{\mathbf{u}}$ spans $\{\hat{\mathbf{x}}, \hat{\mathbf{y}}, \hat{\mathbf{z}}\}$ and where Γ^+ (resp. Γ^-) is a cut of the periodic cell at a constant altitude z with $z > z_g$ (resp. z < 0). Finally, one can deduce the diffraction efficiencies from the transverse components of the field $\mathbf{E} \cdot \hat{\mathbf{x}}$ and $\mathbf{E} \cdot \hat{\mathbf{y}}$ only:

Diffraction efficiencies |

$$\begin{cases}
R_{m,n}^{\parallel} = \frac{1}{\gamma_{m,n}^{r} k_{z,1}} \left[(\gamma_{m,n}^{r}^{2} + \alpha_{m,n}^{2}) |e_{m,n}^{r,x}|^{2} + (\gamma_{m,n}^{r}^{2} + \beta_{m,n}^{2}) |e_{m,n}^{r,y}|^{2} \right. \\
+ 2 \alpha_{m,n} \beta_{m,n} \Re e \left\{ e_{m,n}^{r,x} \overline{e_{m,n}^{r,y}} \right\} \right] \\
T_{m,n}^{\parallel} = \frac{1}{\gamma_{m,n}^{t} k_{z,1}} \left[(\gamma_{m,n}^{t}^{2} + \alpha_{m,n}^{2}) |e_{m,n}^{t,x}|^{2} + (\gamma_{m,n}^{t}^{2} + \beta_{m,n}^{2}) |e_{m,n}^{t,y}|^{2} \right. \\
+ 2 \alpha_{m,n} \beta_{m,n} \Re e \left\{ e_{m,n}^{t,x} \overline{e_{m,n}^{t,y}} \right\} \right]
\end{cases} (2.19)$$

This last expression of the diffraction efficiencies is handy since it does not require to explicitly compute the Rayleigh coefficients $e_{m,n}^{r,z}$ and $e_{m,n}^{t,z}$ involving the normal component of the field on Γ^{\pm} . Indeed, with vector elements defined on edges and faces of tetrahedrons, the (discontinuous) normal component to a surface is not readily available. It can however be retrieved through the use of a Lagrange multiplier (and the **Trace** operator defined in GetDP). Once determined, another formula for the diffraction efficiencies can be used:

Diffraction efficiencies \perp

$$\begin{cases}
R_{m,n}^{\perp} = \frac{1}{\gamma_{m,n}^{r} k_{z,1}} \left[\alpha_{m,n}^{2} |e_{m,n}^{r,x}|^{2} + \beta_{m,n}^{2} |e_{m,n}^{r,y}|^{2} + \gamma_{m,n}^{t} |e_{m,n}^{r,z}|^{2} \right] \\
T_{m,n}^{\perp} = \frac{1}{\gamma_{m,n}^{t} k_{z,1}} \left[\alpha_{m,n}^{2} |e_{m,n}^{t,x}|^{2} + \beta_{m,n}^{2} |e_{m,n}^{t,y}|^{2} + \gamma_{m,n}^{t} |e_{m,n}^{t,z}|^{2} \right]
\end{cases} ,$$
(2.20)

As for the Joule losses whithin an (isotropic) groove region of relative permittivity $\varepsilon_{r,g}(\mathbf{x})$, they can be retrived by computing the following ratio:

Joule Losses

$$Q = \frac{\int_{\Omega_g} \frac{1}{2} \omega \,\varepsilon_0 \,\Im m(\varepsilon_{r,g}) \,|\mathbf{E}|^2 \,\mathrm{d}\Omega}{\int_{\Gamma^+} \frac{1}{2} \Re e\{\mathbf{E}^{\mathrm{inc}} \times \overline{\mathbf{H}^{\mathrm{inc}}}\} \cdot -\hat{\mathbf{z}} \,\mathrm{d}\Gamma}.$$
 (2.21)

The numerator in Eq. (2.21) clarifies losses in watts by bi-period of the considered crossedgrating and are computed by integrating the Joule effect losses density over the volume V of the lossy element. The denominator normalizes these losses to the incident power, *i.e.* the time-averaged incident Poynting vector flux across one bi-period. Since \mathbf{E}^{inc} is nothing but a plane wave, this last term is equal to $A_e^2/2\sqrt{\varepsilon_{r,1}\varepsilon_0/\mu_0} d_x d_y \cos \xi \cos \theta_0$.

2.6 Total field formulation

It should be stated that for gratings, it is relatively easy to implement a total field formulation of the problem using a virtual antenna on Γ^+ . The induced current to impose on the surface is equal $2\hat{\mathbf{z}} \times \mathbf{H}_1$ [Jin15; Str07], which is handled through a Robin condition on Γ^+ :

$$-\int_{\Omega} \boldsymbol{\mu}_{r}^{-1} \operatorname{\mathbf{curl}} \mathbf{E} \cdot \overline{\operatorname{\mathbf{curl}} \mathbf{W}} d\Omega + k_{0}^{2} \int_{\Omega} \boldsymbol{\varepsilon}_{r} \mathbf{E} \cdot \overline{\mathbf{W}} d\Omega$$

$$-2i\omega \mu_{0} \int_{\Gamma^{+}} (\hat{\mathbf{z}} \times \mathbf{H}_{1}) \cdot \overline{\mathbf{W}} d\Gamma$$

$$=0,$$
(2.22)

for an amagnetic problem with homogeneous Neumann conditions at PMLs endings, which allows to disregard the last three terms of the formulation in Eq. 2.16. The assembly time of the total field formulation is slightly shorter than the scattered field one due to the presence of surface source term instead of a volume one. However, the implementation remains of the same level of difficulty as in the scattered field one since the annex problem still has to be solved in order to compute the annex magnetic field \mathbf{H}_1 .

2.7 Convergence

The convergence of the energy related quantities with respect to the mesh refinement and finite element order can easily be checked using the grating3D.pro model. Running gmsh grating3D.pro -setstring test_case convergence from the command line allows to retrieve all the results presented in Fig. 2.2. This test case loops over the mesh refinement parametrized by N, the approximate number of tetrahedra per wavelength in a given material (i.e. the mesh size is set to $\lambda_0/(N\sqrt{\varepsilon_r})$), and the interpolation order.

The blue and orange curves in Fig. 2.2(a) show the specular transmitted efficiency $T_{0,0}^{\parallel}$ (see Eq. 2.19) as a function of N. These curves are superimposed with the green and blue ones representing $T_{0,0}^{\perp}$ (see Eq. 2.20). The purple, brown, pink and grey curves represent the same quantities as described just before, when computed using the total field formulation described in Sec. 2.6. The convergence rate is shown in Fig. 2.2(b). The corresponding number of unknowns, direct solver runtime and allocated RAM are indicated in Figs. 2.2(c-e).

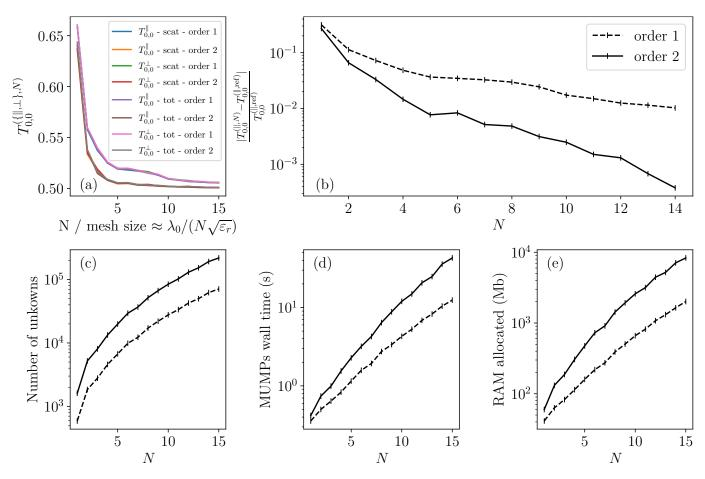


Figure 2.2: (a) Convergence of $T_{0,0}^{\parallel}$ (Eq. 2.19) and $T_{0,0}^{\perp}$ (Eq. 2.20) as a function of the formulation type (scattered or total), interpolation order and mesh refinement parametrized by N, the number of mesh elements per wavelength in a given material. (b) Convergence rate as a function of the mesh refinement and the interpolation order. The reference value $T_{0,0}^{(\parallel,\text{ref})}$ is the one obtained with second order and N=15. (c) Number of unknowns as a function of the mesh refinement. (d) Direct solver wall time in seconds. (e) Allocated RAM.

Chapter 3

The conical 2.5D case

The conventions and notations adopted for the conical incidence case, or 2.5D case, are shown in Fig. 3.1 where a 3D plane wave is incident on a 2D geometry. Note that the coordinate system has changed $(x \to z, y \to x, z \to y)$ from the 3D case in order to match the more usual convention where (Oz) is the geometrical axis of invariance. The conical case can be tackled using a mixed formulation [Zol+12], where the possibly discontinuous transverse components of the unknown field, denoted by $\mathbf{E}^d_{2,t} := E^d_{2,x}(x,y)\hat{\mathbf{x}} + E^d_{2,y}(x,y)\hat{\mathbf{y}}$, are discretized with edge elements and the continuous longitudinal component denoted $E^d_{2,z}(x,y)$ by nodal elements.

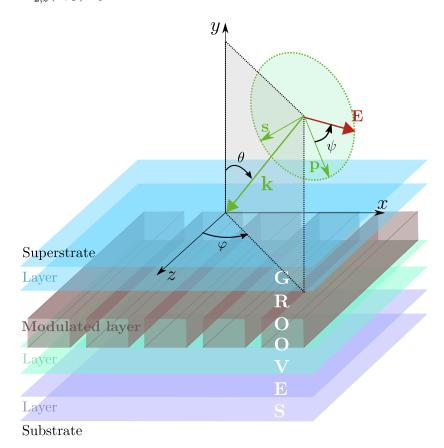


Figure 3.1: Convention and notation for the conical case.

The following handy transverse operators \mathbf{grad}_t and \mathbf{curl}_t are introduced:

$$\operatorname{\mathbf{grad}}_t f = \partial_x f \,\hat{\mathbf{x}} + \partial_y f \,\hat{\mathbf{y}} \text{ and } \operatorname{\mathbf{curl}}_t \mathbf{F} = (\partial_y F_x - \partial_x F_y) \,\hat{\mathbf{z}}.$$

Restricting the generality of the relative permittivity (and permeability) tensors in the following way:

$$\boldsymbol{\varepsilon}_{r} = \begin{bmatrix} \varepsilon_{r,xx} & \overline{\varepsilon_{r,a}} & 0\\ \varepsilon_{r,a} & \varepsilon_{r,yy} & 0\\ 0 & 0 & \varepsilon_{r,zz} \end{bmatrix} = \underbrace{\begin{bmatrix} \varepsilon_{r,xx} & \overline{\varepsilon_{r,a}} & 0\\ \varepsilon_{r,a} & \varepsilon_{r,yy} & 0\\ 0 & 0 & 1 \end{bmatrix}}_{\boldsymbol{\widetilde{\varepsilon}}_{r}} \begin{bmatrix} 1 & 0 & 0\\ 0 & 1 & 0\\ 0 & 0 & \varepsilon_{r,zz} \end{bmatrix}$$
(3.1)

allows to convieniently decouple the tranverse and longitudinal behavior of the field. Indeed, we are looking for a solution of the scattering problem under the form of the following ansatz $\mathbf{E}_2^{\mathrm{d}} = \left[\mathbf{E}_{2,t}^d(x,y) + E_{2,z}(x,y)\,\hat{\mathbf{z}}\right]e^{ik_zz}$, where k_z is the longitudinal component of the incident wavevector. Thus, the decoupling mentionned above writes:

$$\boldsymbol{\mu}_r^{-1}\mathbf{curl}\,\mathbf{E}_2^{\mathrm{d}} = \left[\mu_{r,zz}^{-1}\mathbf{curl}_t\,\mathbf{E}_{2,t}^d + \tilde{\boldsymbol{\mu}}_r^{-1}(\mathbf{grad}_t\,E_{2,z}^d - ik_z\mathbf{E}_{2,t}^d) \times \hat{\mathbf{z}}\right]e^{ik_zz}$$

Finally, one can obtain the variational formulation for the conical case:

$$\int_{\Omega} \mu_{r,zz}^{-1} \operatorname{\mathbf{curl}}_{t} \mathbf{E}_{2,t}^{d} \cdot \overline{\operatorname{\mathbf{curl}}_{t} \mathbf{W}} d\Omega
+ \int_{\Omega} \left(\tilde{\boldsymbol{\mu}}_{r}^{-1} \left(\hat{\mathbf{z}} \times \operatorname{\mathbf{grad}}_{t} E_{2,z}^{d} \right) \right) \cdot \overline{\hat{\mathbf{z}} \times \operatorname{\mathbf{grad}}_{t} w} d\Omega
+ ik_{z} \int_{\Omega} \left(\tilde{\boldsymbol{\mu}}_{r}^{-1} \left(\hat{\mathbf{z}} \times \operatorname{\mathbf{grad}}_{t} E_{2,z}^{d} \right) \right) \cdot \overline{\hat{\mathbf{z}} \times \mathbf{W}} d\Omega
- ik_{z} \int_{\Omega} \left(\tilde{\boldsymbol{\mu}}_{r}^{-1} \left(\hat{\mathbf{z}} \times \mathbf{E}_{2,t}^{d} \right) \right) \cdot \overline{\hat{\mathbf{z}} \times \operatorname{\mathbf{grad}}_{t} w} d\Omega
+ k_{z}^{2} \int_{\Omega} \left(\tilde{\boldsymbol{\mu}}_{r}^{-1} \left(\hat{\mathbf{z}} \times \mathbf{E}_{2,t}^{d} \right) \right) \cdot \overline{\hat{\mathbf{z}} \times \mathbf{W}} d\Omega
- k_{0}^{2} \int_{\Omega} \tilde{\boldsymbol{\varepsilon}}_{r} \mathbf{E}_{2,t}^{d} \cdot \overline{\mathbf{W}} d\Omega - k_{0}^{2} \int_{\Omega} \varepsilon_{r,zz} E_{2,z}^{d} \cdot \overline{w} d\Omega + \mathbf{B}.\mathbf{T}.
+ k_{0}^{2} \int_{\Omega_{q}} (\tilde{\boldsymbol{\varepsilon}}_{r,a} - \tilde{\boldsymbol{\varepsilon}}_{r}) \mathbf{E}_{1,t} \cdot \overline{\mathbf{W}} d\Omega + k_{0}^{2} \int_{\Omega_{q}} (\varepsilon_{r,a,zz} - \varepsilon_{r,zz}) E_{1,z} \cdot \overline{w} d\Omega = 0,$$

where B.T. is the boundary term arising from the integration by part of the **curl** operator. As a validation, the same conical configuration is computed using the full 3D formulation (Fig. 3.2(b)) and with the 2.5D conical formulation (Fig. 3.2(b)). The grating is made of silver on a silver substrate and the plane wave angles are in both cases $\theta_0 = 30^\circ$, $\varphi_0 = 30^\circ$ and $\psi_0 = 10^\circ$. All the parameters can be found in the ONELAB template models grating2D.pro and grating3D.pro. The 3D case can be reproduced by command line: gmsh grating3D.pro -setstring test_case retrieve_2D_lamellar or by opening grating3D.pro in Gmsh and selecting retrieve_2D_lamellar in the Geometry dropdown menu. The 2D conical case can be reproduced by command line: gmsh grating2D.pro -setstring test_case LamellarGrating -setnumber flag_polar 2 or by opening grating2D.pro in Gmsh and selecting LamellarGrating in the Geometry drop-down menu and conical in the polarization case drop-down menu.

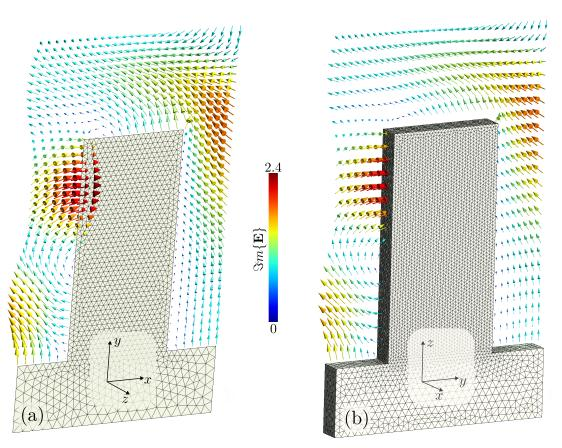


Figure 3.2: Total electric field obtained with the conical model (a) and with the 3D model (b).

Bibliography

- [Dem+07] Guillaume Demésy et al. "The finite element method as applied to the diffraction by an anisotropic grating". In: *Opt. Express* 15.26 (Dec. 2007), pp. 18089–18102. DOI: 10. 1364/0E.15.018089.
- [Dem+09] Guillaume Demésy et al. "Versatile full-vectorial finite element model for crossed gratings". In: Opt. Lett. 34.14 (July 2009), pp. 2216–2218. DOI: 10.1364/OL.34.002216.
- [Dem+10] Guillaume Demésy et al. "All-purpose finite element formulation for arbitrarily shaped crossed-gratings embedded in a multilayered stack". In: *J. Opt. Soc. Am. A* 27.4 (Apr. 2010), pp. 878–889. DOI: 10.1364/JOSAA.27.000878.
- [Dul+98] P. Dular et al. "A general environment for the treatment of discrete problems and its application to the finite element method". In: *IEEE Transactions on Magnetics* 34.5 (1998), pp. 3395–3398.
- [Feh+02] Anne-Laure Fehrembach, Daniel Maystre, and Anne Sentenac. "Phenomenological theory of filtering by resonant dielectric gratings". In: JOSA A 19.6 (2002), pp. 1136–1144.
- [Geu+09] C. Geuzaine and J.-F. Remacle. "Gmsh: a three-dimensional finite element mesh generator with built-in pre- and post-processing facilities". In: *International Journal for Numerical Methods in Engineering* 79.11 (2009), pp. 1309–1331.
- [Gra99] Gérard Granet. "Reformulation of the lamellar grating problem through the concept of adaptive spatial resolution". In: *JOSA A* 16.10 (1999), pp. 2510–2516.
- [Jin15] Jian-Ming Jin. The finite element method in electromagnetics. John Wiley & Sons, 2015.
- [Joh+72] P. B. Johnson and R. W. Christy. "Optical Constants of the Noble Metals". In: *Physical Review B* 6.12 (Dec. 1972), pp. 4370-4379. DOI: 10.1103/PhysRevB.6.4370. URL: http://link.aps.org/doi/10.1103/PhysRevB.6.4370.
- [Pal98] Edward D Palik. Handbook of optical constants of solids. Vol. 3. Academic press, 1998.
- [Pet80] Roger Petit. "Electromagnetic Theory of Gratings". In: Electromagnetic Theory of Gratings. Series: Topics in Current Physics 22 (1980).
- [Pet92] R. Petit. Ondes électromagnétiques en radioélectricité et en optique. fr. Masson, 1992. ISBN: 978-2-225-81571-3.
- [Pol] Mikhail Polyanskiy. URL: https://refractiveindex.info/ (visited on 11/01/2022).
- [Str07] Julius Adams Stratton. *Electromagnetic theory*. Vol. 33. John Wiley & Sons, 2007.
- [Zol+12] Frédéric Zolla et al. Foundations of Photonic Crystal Fibres. 2nd. Imperial College Press, 2012.